

Realistic non-local refrigeration engine based on Coulomb coupled systems

Anamika Barman, Surojit Halder, Shailendra K. Varshney, Gourab Dutta, and Aniket Singha
*Department of Electronics and Electrical Communication Engineering,
 Indian Institute of Technology Kharagpur,
 Kharagpur-721302, India*

Employing Coulomb-coupled systems, we demonstrate a cryogenic non-local refrigeration engine, that circumvents the need for a change in the energy resolved system-to-reservoir coupling, demanded by the recently proposed non-local refrigerators [1–5]. We demonstrate that an intentionally introduced energy difference between the ground states of adjacent tunnel coupled quantum dots, associated with Coulomb coupling, is sufficient to extract heat from a remote target reservoir. Investigating the performance and operating regime using quantum-master-equation (QME) approach, we point out to some crucial aspects of the proposed refrigeration engine. In particular, we demonstrate that the maximum cooling power for the proposed set-up is limited to about 70% of the optimal design. Proceeding further, we point out that to achieve a target reservoir temperature, lower compared to the average temperature of the current path, the applied voltage must be greater than a given threshold voltage V_{TH} , that increases with decrease in the target reservoir temperature. In addition, we demonstrate that the maximum cooling power, as well as the coefficient of performance deteriorates as one approaches a lower target reservoir temperature. The novelty of the proposed refrigeration engine is the integration of fabrication simplicity along with descent cooling power. The idea proposed in this paper may pave the way towards the realization of efficient non-local cryogenic refrigeration systems.

I. INTRODUCTION

With scaling technology rapidly invading the nano-domain, the tremendous rise in dissipated heat density and hence operating temperature has drawn significant attention towards electrical refrigeration in nano-scale dimensions [1–22]. In addition, sophisticated experiments on exploratory technologies, such as quantum computation, spin and optics based computation, etc. occasionally call for electrical refrigeration at cryogenic temperatures in nano-meter range length scale. However, the refrigeration performance in such nano-scale systems is often affected drastically by the large lattice heat flux, particularly when both the region of refrigeration and heat dissipation lie along the path of current flow and are separated by a few nanometres in space. Despite lots of effort to reduce lattice thermal conductance [23–34], the performance of nano refrigeration systems is still affected by rapid reverse heat flux. This effect poses a threat to the refrigeration performance as device channels are gradually invading the nano-domain. An attempt to improve the refrigeration performance by engineering lattice thermal conductance generally deteriorates the electronic conductivity and hence the cooling power. As an alternative, one of the major research focus, concerning nano-scale refrigeration engine, is to facilitate an independent manipulation of the electron transport path and lattice heat conduction path, by introducing a spatial separation between the current path and the target reservoir [1–5, 35–37]. This phenomenon of refrigerating a remote target reservoir, which is spatially separated from the current track, is known as non-local refrigeration [1–5, 35–37]. Thus, non-local refrigeration systems are three terminal systems where input power is delivered between

two terminals to extract heat from a remote target reservoir through the third terminal. In this case, optimizing the lattice heat transport path, in an attempt to improve refrigeration performance, can be accomplished without modifying the current conduction path. These kind of systems, thus enables an independent optimization of the lattice thermal conductance and the current conductivity [1–5, 35–37]. In addition, due to the non-locality of the electronic transport path, the refrigerated region is significantly shielded from reverse heat flux owing to the Joule dissipation.

Recently, optimal non-local refrigeration systems based on Coulomb coupled quantum dots have been proposed and explored in the literature [1–5]. However, the operation of these refrigeration engines call for a sharp step-like change in the energy-resolved system-to-reservoir coupling around the quantum-dot ground state [1–5], which is impossible to achieve in realistic systems. In this paper, we propose a design strategy for non-local refrigeration using Coulomb coupled systems, that can operate optimally without demanding a sharp transition in the system-to-reservoir coupling. The refrigeration engine is then theoretically analyzed using quantum master equation (QME) approach for such systems in the sequential tunneling limit [38]. It is demonstrated that the maximum cooling power (heat extracted per unit time) for the proposed design is limited to about 70% of that for the optimal design [1–5]. Despite of a lower performance compared to the optimal set-up, the novelty of the proposed design lies in the integration of fabrication simplicity along with a decent cooling power, making such design suitable for practical applications. At the end, the sequential transport phenomena leading to a deterioration of performance of the proposed set-up is investigated

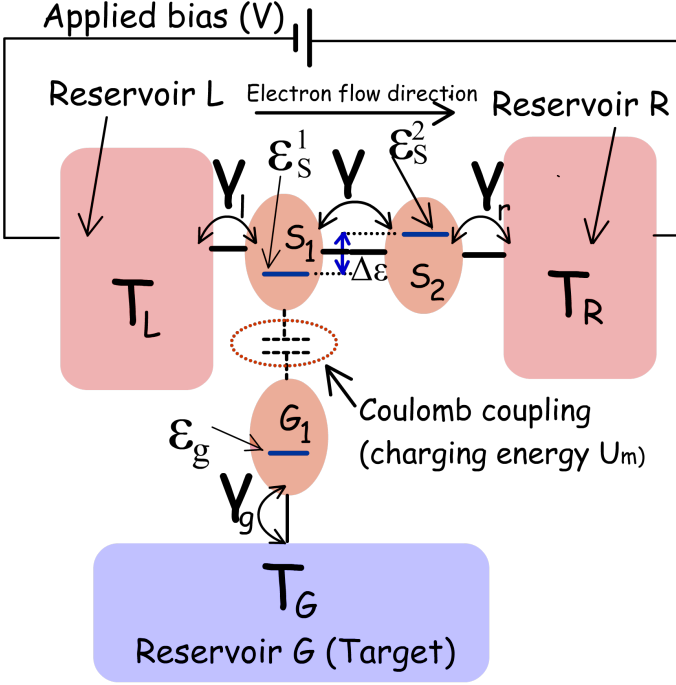


FIG. 1. Schematic of the proposed non-local refrigeration engine employing Coulomb coupled systems. The system consists of three dots- S_1 , S_2 and G_1 , which are electrically coupled to the macroscopic electron reservoirs L , R and G respectively. S_1 is tunnel coupled to S_2 and capacitively coupled to G_1 . The tunnel coupled quantum dots S_1 and S_2 share a stair-case ground state configuration with $\varepsilon_s^2 = \varepsilon_s^1 + \Delta\varepsilon$.

and a strategy to alleviate such transport processes is presented.

The paper is organized as follows. In Sec. II, we briefly describe the proposed design along with the transport formulation employed to analyze the performance of the refrigeration engine. In the following Sec. III, we investigate the performance and region of operation of the proposed refrigeration engine for two different cases (i) $T_G < T_{L(R)}$ and $T_G = T_{L(R)}$. This section also presents a performance comparison of the proposed refrigeration engine with the optimal set-up proposed in literature [1–5], in addition to an investigation of the sequential processes leading to a performance deterioration of the proposed set-up. Finally, we conclude this paper briefly in Sec. IV.

II. PROPOSED DESIGN AND TRANSPORT FORMULATION

The proposed non-local refrigeration engine is schematically illustrated in Fig. 1, where three quantum dots S_1 , S_2 and G_1 are electrically coupled with electronic reservoirs L , R and G respectively, G being the target reservoir to be refrigerated. S_1 and S_2 are tunnel coupled to each other, while G_1 is capacitively coupled to S_1 by suitable fabrication techniques. The

capacitive coupling between S_1 and G_1 permits energy exchange while obstructing any particle swap between the dots. In the optimal Coulomb-coupled system based refrigeration-engine, an asymmetric system-to-reservoir coupling is required for refrigeration [1, 5]. In the proposed set-up, on the other hand, the asymmetry, with respect to the reservoir L and R , is embedded within the system itself by choosing a difference between the ground states of the tunnel-coupled quantum dots S_1 and S_2 , with $\varepsilon_s^2 = \varepsilon_s^1 + \Delta\varepsilon$. The electrically coupled dots S_1 and S_2 may be suitably fabricated or gated to retain a stair-case ground-state configuration with $\varepsilon_s^2 = \varepsilon_s^1 + \Delta\varepsilon$. We will demonstrate via numerical calculations and theoretical arguments that in the system detailed above, refrigeration of the target reservoir G can be achieved by forcing a net electronic flow from L to R , that is, refrigeration can be achieved at a terminal non-local to the current path. The excess energy $\Delta\varepsilon = \varepsilon_s^2 - \varepsilon_s^1$, required for the electrons to tunnel from S_1 to S_2 is extracted from the reservoir G via Coulomb coupling. Coming to the fabrication feasibility of such a system, due to the recent progress in nano-fabrication techniques, coupled systems employing multiple (more than two) quantum dots, with and without Coulomb coupling, have already been experimentally realized [39–44]. In addition, it has been experimentally demonstrated that spatially and electrically isolated quantum dots may be bridged to obtain strong Coulomb coupling, in addition to excellent thermal insulation [45–49]. In addition, the bridge may be constructed between two specific dots to radically increase their mutual Coulomb coupling, without affecting the electrostatic potential of the other quantum dots [45–49]. Thus, the fluctuation in electron number n_{S_1} (n_{G_1}) of the dot S_1 (G_1) alters the electrostatic energy of the dot G_1 (S_1). The total increase in electrostatic energy U of the configuration, consisting of three dots, due to fluctuation in electron number can be given by [38, 50]:

$$U(n_{S_1}, n_{G_1}, n_{S_2}) = \sum_x U_x^{self} (n_x^{tot} - n_x^{eq})^2 + \sum_{\substack{x_1 \neq x_2 \\ (x_1, x_2)}} U_{x_1, x_2}^m (n_{x_1}^{tot} - n_{x_1}^{eq}) (n_{x_2}^{tot} - n_{x_2}^{eq})$$

where n_x^{tot} is the total electron number at finite temperature, and n_x^{eq} is the total electron number under equilibrium conditions at $0K$ in the dot x (satisfying the condition that the system equilibrates at the minimum possible value of electrostatic energy at $0K$). $U_x^{self} = \frac{q^2}{C_x^{self}}$ is the electrostatic energy due to self-capacitance C_x^{self} (with the adjacent terminals) of quantum dot x and U_{x_1, x_2}^m is the mutual electrostatic energy between two spatially separated quantum dots x_1 and x_2 . $n_x = n_x^{tot} - n_x^{eq}$ is the number of excess electrons in the ground state of dot x due to thermal fluctuations (kicks) from the reservoirs at finite temperature. To investigate the performance of the refrigeration engine, we consider a minimal physics-based model to simplify our calculations. We assume that the electrostatic energy due to self-capacitance is much greater than the applied voltage V or the average thermal voltage kT/q , i.e. $U_x^{self} \gg (kT, qV)$, where $T = \frac{T_{L(R)} + T_G}{2}$, such that electron occupancy probability or transfer rate across the Coulomb blocked energy

level due to self-capacitance is negligibly small. Hence, the ground state of a particular dot can be occupied by atmost one electron and the behaviour of the entire system can be analyzed via $2^3 = 8$ different multi-electron states. These states may be denoted as $|n_{S_1}, n_{G_1}, n_{S_2}\rangle = |n_{S_1}\rangle \otimes |n_{G_1}\rangle \otimes |n_{S_2}\rangle$ where $n_{S_1}, n_{G_1}, n_{S_2} \in (0, 1)$ indicate the number of electrons in the ground state of S_1, G_1 and S_2 respectively. We consider that the Coulomb coupling between $S_1 - S_2$ and $S_2 - G_1$ is negligible compared to the relevant energy scales of the system, that is, electrostatic coupling between S_1, S_2 , and S_2, G_1 is negligible with respect to U_{S_1, G_1}^m, kT and qV . Thus, for all practical purpose relating to electron transport $U_{S_1, S_2}^m \approx 0$ and $U_{G_1, S_2}^m \approx 0$. Due to capacitive coupling, the electronic transport through S_1 and G_1 are interdependent, and hence, the pair of dots S_1 and G_1 are treated as a

sub-system (ς_1) of the entire system, S_2 being the complementary sub-system labeled as ς_2 [38]. The probability of the sub-system (ς_1) to be in a particular state is denoted by $P_{i,j}^{\varsigma_1}$, where i and j are the number of electrons in the ground state of the dots S_1 and G_1 respectively. On the other hand, $P_k^{\varsigma_2}$ denotes the steady-state occupancy probability of dot S_2 (subsystem ς_2). Under the condition that $\Delta\varepsilon$ is much higher than the ground state broadening due to reservoir coupling, the optimal inter-dot tunneling between S_1 and S_2 occurs when $\Delta\varepsilon = U_{S_1, G_1}^m$, such that $\varepsilon_s^2 = (\varepsilon_s^1 + U_{S_1, G_1}^m)$ [38]. Hence, for the optimal performance investigation of the proposed set-up, we assume $\Delta\varepsilon = U_{S_1, G_1}^m$. In what follows, we simply refer to U_{S_1, G_1}^m as U_m to make the notations compact. With all the above assumptions, the equations dictating the steady state sub-system probabilities can be obtained as follows [38]:

$$\begin{aligned} & -P_{0,0}^{\varsigma_1}\{f_L(\varepsilon_s^1) + f_G(\varepsilon_g^1)\} + P_{0,1}^{\varsigma_1}\{1 - f_G(\varepsilon_g^1)\} + P_{1,0}^{\varsigma_1}\{1 - f_L(\varepsilon_s^1)\} = 0 \\ & -P_{1,0}^{\varsigma_1}\{1 - f_L(\varepsilon_s^1) + f_G(\varepsilon_g^1 + U_m)\} + P_{1,1}^{\varsigma_1}\{1 - f_G(\varepsilon_g^1 + U_m)\} + P_{0,0}^{\varsigma_1}f_L(\varepsilon_s^1) = 0 \\ & -P_{0,1}^{\varsigma_1}\left\{1 - f_G(\varepsilon_g^1) + f_L(\varepsilon_s^1 + U_m) + \frac{\gamma}{\gamma_c}P_1^{\varsigma_2}\right\} + P_{0,0}^{\varsigma_1}f_G(\varepsilon_g^1) + P_{1,1}^{\varsigma_1}\left\{1 - f_L(\varepsilon_s^1 + U_m) + \frac{\gamma}{\gamma_c}P_1^{\varsigma_2}\right\} = 0 \\ & -P_{1,1}^{\varsigma_1}\left\{[1 - f_G(\varepsilon_g^1 + U_m)] + [1 - f_L(\varepsilon_s^1 + U_m)] + \frac{\gamma}{\gamma_c}P_0^{\varsigma_2}\right\} + P_{1,0}^{\varsigma_1}f_G(\varepsilon_g^1 + U_m) + P_{0,1}^{\varsigma_1}\left\{f_L(\varepsilon_s^1 + U_m) + \frac{\gamma}{\gamma_c}P_1^{\varsigma_2}\right\} = 0 \quad (1) \end{aligned}$$

$$\begin{aligned} & -P_0^{\varsigma_2}\{f_R(\varepsilon_s^2) + \frac{\gamma}{\gamma_c}P_{1,1}^{\varsigma_1}\} + P_1^{\varsigma_2}\left\{1 - f_R(\varepsilon_s^2) + \frac{\gamma}{\gamma_c}P_{0,1}^{\varsigma_1}\right\} = 0 \\ & -P_1^{\varsigma_2}\{1 - f_R(\varepsilon_s^2) + \frac{\gamma}{\gamma_c}P_{0,1}^{\varsigma_1}\} + P_0^{\varsigma_2}\left\{f_R(\varepsilon_s^2) + \frac{\gamma}{\gamma_c}P_{1,1}^{\varsigma_1}\right\} = 0, \quad (2) \end{aligned}$$

where γ and γ_c are the associated rates of inter-dot tunneling and system to reservoir tunneling respectively [38, 50, 51]. and $f_\zeta(\epsilon)$ is the statistical occupancy probability of the reservoir ζ at energy ϵ . For the purpose of our present calculations, we assume quasi-equilibrium electron statistics at the reservoir and hence the function $f_\zeta(\epsilon)$ is the Fermi-Dirac function for the corresponding quasi-Fermi level at reservoir ζ .

$$f_\zeta(\epsilon) = \left\{1 + \exp\left(\frac{\epsilon - \mu_\zeta}{kT_\zeta}\right)\right\}^{-1}, \quad (3)$$

where T_ζ and μ_ζ are the temperature and quasi-Fermi energy of the reservoir ζ respectively. The group of Eqs. (1) and (2) signify that interdot electron transport between S_1 and S_2 can only occur when the ground state of G_1 is occupied. Both (1) and (2) form dependent sets of equations, which can be broken by employing the probability conservation rules $\sum_{i,j=0,1} P_{i,j}^{\varsigma_1} = 1$ and $\sum_{k=0,1} P_k^{\varsigma_2} = 1$. The sets of Eqs. (1) and (2) form a non-linear set of equations and should be solved using any iterative numerical method. For the purpose of our present calculation, Newton-Raphson scheme was used to calculate the system steady-state probabilities $P_{i,j}^{\varsigma_1}$ and $P_k^{\varsigma_2}$. On calculation of steady-state probabilities

the charge current between the system and the reservoirs $I_{L(R)}$ and the heat current I_{Qe} (extracted from the reservoir G) can be calculated as:

$$\begin{aligned} I_L &= q\gamma_c \times \{P_{0,0}^{\varsigma_1}f_L(\varepsilon_s^1) + P_{0,1}^{\varsigma_1}f_L(\varepsilon_s^1 + U_m)\} \\ &\quad - q\gamma_c P_{1,0}^{\varsigma_1}\{1 - f_L(\varepsilon_s^1)\} - q\gamma_c P_{1,1}^{\varsigma_1}\{1 - f_L(\varepsilon_s^1 + U_m)\} \quad (4) \end{aligned}$$

$$I_R = -q\gamma_c \times \{P_0^{\varsigma_2}f_R(\varepsilon_s^1) - P_1^{\varsigma_2}\{1 - f_R(\varepsilon_s^1)\}\}, \quad (5)$$

$$I_{Qe} = U_m\gamma_c \{P_{1,0}^{\varsigma_1}f_G(\varepsilon_g + U_m) - P_{1,1}^{\varsigma_1}\{1 - f_G(\varepsilon_g + U_m)\}\} \quad (6)$$

In Eq. (6), we have neglected the reverse heat flux due to lattice thermal conductivity, assuming ideal thermal insulation of the reservoir G with its surroundings. It should be noted that, the heat extracted per unit time from reservoir G , given in Eq. (6), is not directly dependent on the ground state ε_g of G_1 due to the fact that the net current into (or out of) reservoir G is zero. As described, to achieve refrigeration in the reservoir G , a net electronic flow has to be injected from L to R . To achieve such electron flow, a voltage bias can be applied between L and R with the negative and positive terminals of the bias connected to the terminals L and R respectively. We now briefly discuss the electronic transport processes resulting in the refrigeration of the reservoir G . Let us consider that the system is in the initial state $|0, 0, 0\rangle$, which we also call as the vacuum state. A sequence of electronic transport that extracts a heat packet U_m from the reservoir G is as follows: $|0, 0, 0\rangle \rightarrow |1, 0, 0\rangle \rightarrow |1, 1, 0\rangle \rightarrow$

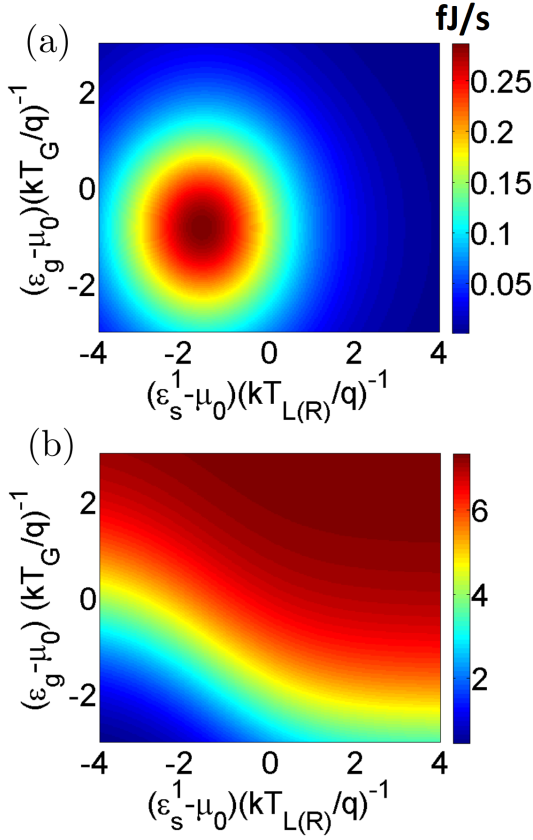


FIG. 2. Regime of refrigeration of the proposed design for low bias condition ($V = 0.2 \frac{kT}{q}$) with $T_L = T_R = T_G = T = 10K$. Color plots are showing the variation of (a) cooling power (I_{Qe}) and (b) COP with the position of the ground states ϵ_g and ϵ_s^1 for $V = 0.2 \frac{kT}{q}$ ($\approx 0.17meV$) and $U_m = 3 \frac{kT}{q}$ ($\approx 2.5meV$).

$|0, 1, 1\rangle \rightarrow |0, 1, 0\rangle \rightarrow |0, 0, 0\rangle$. In this sequence, the system starts with the vacuum state. Next, an electron is injected into S_1 with an energy ϵ_s^1 followed by an electron injection in G_1 with an energy $\epsilon_g + U_m$. Next, the electron in S_1 gets transferred to S_2 via interdot tunneling and subsequently flows out of the terminal R . The system returns to the initial vacuum state when the electron in G_1 tunnels out to G with an energy ϵ_g . Note that in this cycle, the electron is injected into G_1 from G with energy $\epsilon_g + U_m$ and extracted back into G with energy ϵ_g . Thus, the reservoir G loses a packet of heat energy U_m . Such a transport process and other equivalent sequential processes lead to a refrigeration in the reservoir G .

When analyzing the refrigeration performance, two parameters of prime importance constitute the cooling power or the heat extracted per unit time I_{Qe} (defined in Eq. (6)) and the heat extracted per unit input power, which is also known as the coefficient of performance (COP) of the refrigerator. The total input power (P) is dependent on the bias voltage as well as the injected

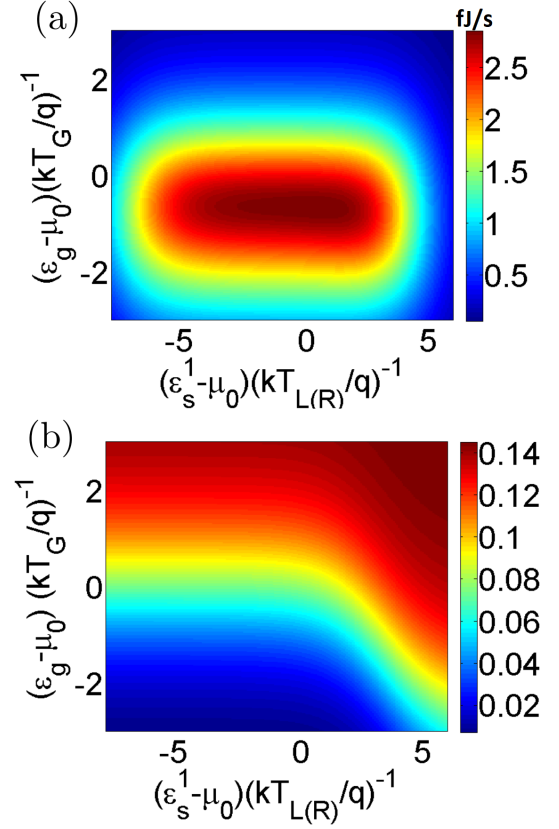


FIG. 3. Regime of refrigeration of the proposed design for high bias condition ($V = 10 \frac{kT}{q}$) with $T_L = T_R = T_G = T = 10K$. Color plots are showing the variation of (a) cooling power (I_{Qe}) and (b) COP with the position of the ground states ϵ_g and ϵ_s^1 for $V = 10 \frac{kT}{q}$ ($\approx 8.5meV$) and $U_m = 3 \frac{kT}{q}$ ($\approx 2.5meV$).

current and can be defined as:

$$P = I_{L(R)} \times V, \quad (7)$$

where V is the applied bias voltage across the reservoir L and R . As stated above, the efficiency of a refrigerator is normally characterized by its coefficient of performance (COP):

$$COP = \frac{I_{Qe}}{P}, \quad (8)$$

where the heat extracted per unit time from G can be calculated using Eq. (6).

III. RESULTS

In this section, we describe the operation regime of the proposed refrigeration engine. In addition, we also compare the performance of our design with the optimal non-local refrigerator discussed in literature and elaborate the transport processes dominating the proposed set-up.

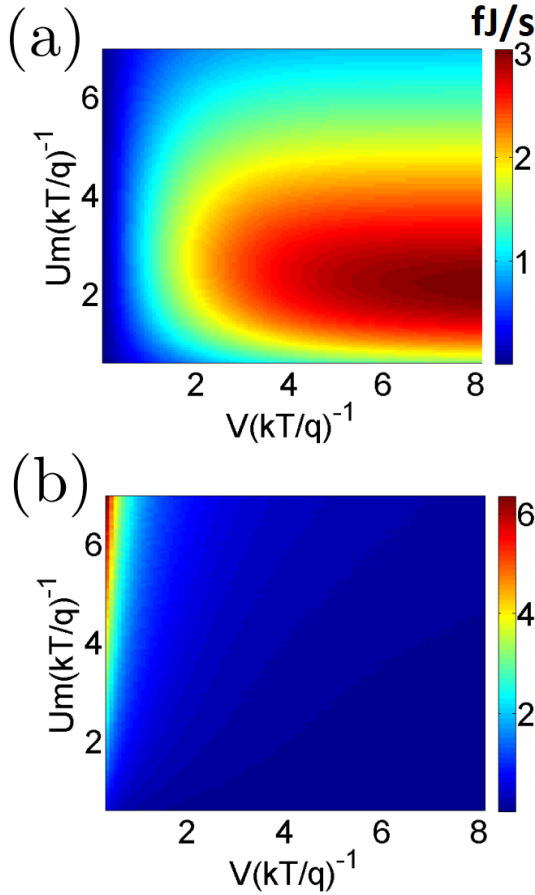


FIG. 4. Variation in refrigeration performance of the proposed set-up for with $T_{L(R)} = 10K$ and $T_G = 10K$. Color plots are showing the variation of (a) maximum cooling power $I_{Q_e}^M$ and (b) COP at the maximum cooling power with the applied bias voltage V and Coulomb coupling energy U_m . To find out the maximum cooling power for a given value of V and U_m , the ground states of the dots are tuned to their optimal position. $T = \frac{T_{L(R)} + T_G}{2}$ is the average temperature between the hot and the cold reservoirs.

Without loss of generality, we assume that $\gamma_c = 10^{-6} \frac{q}{h}$ and $\gamma = 10^{-5} \frac{q}{h}$.

Analysis of performance and regime of operation: Fig. 2 and 3 demonstrate the operation regime of the refrigeration engine for low bias ($V = 0.2 \frac{kT}{q}$) and high bias ($V = 10 \frac{kT}{q}$) condition respectively for Coulomb coupling energy $U_m = 3 \frac{kT}{q}$ and $T_{L(R)} = T_G = T = 10K$. In particular, Fig. 2(a) and (b) demonstrate the cooling power I_{Q_e} and COP respectively over a range of the ground state positions for ε_s^1 and ε_g . It can be noted from Fig. 2(a) that the regime of refrigeration corresponds to ε_s^1 lying within a few kT around μ_0 , that is $-few kT < \varepsilon_s^1 - \mu_0 < few kT$. Such a trend occurs since the rate of electron transport through the system, under low bias condition, peaks when the ground states of the quantum dots lie within a few kT of the equilib-

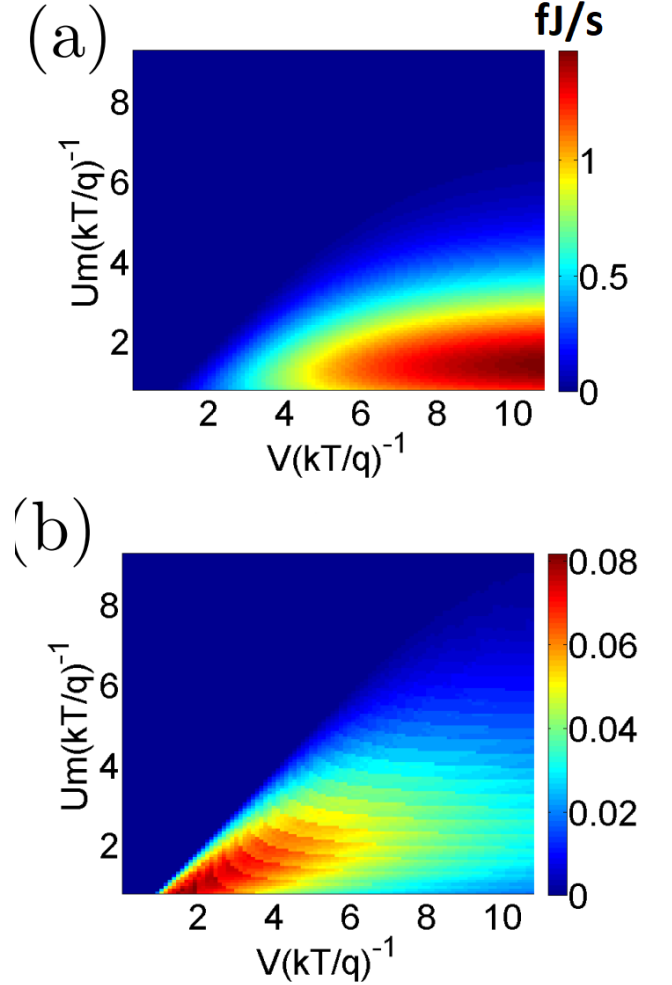


FIG. 5. Variation in refrigeration performance of the proposed set-up for with $T_{L(R)} = 10K$ and $T_G = 5K$. Color plots are showing the variation of (a) maximum cooling power $I_{Q_e}^M$ and (b) COP at the maximum cooling power with the applied bias voltage V and Coulomb coupling energy U_m . To find out the maximum cooling power for a given value of V and U_m , the ground states of the dots are tuned to their optimal position. $T = \frac{T_{L(R)} + T_G}{2}$ is the average temperature between the hot and the cold reservoirs.

rium Fermi-energy μ_0 . We also note that the refrigeration power is finite and large when the ε_g lies within a few kT of the equilibrium Fermi energy μ_0 , that is, when $-few kT < \varepsilon_g - \mu_0 < few kT$. Such a behaviour occurs due to the fact that for extraction of heat energy from G , an electron must be able to tunnel into and out of G_1 with energy $\varepsilon_g + U_m$ and ε_g respectively. Hence, both the functions $f_G(\varepsilon_g + U_m)$ and $1 - f_G(\varepsilon_g)$ must have finite values which is only possible if ε_g lies within a few kT of the equilibrium Fermi-energy μ_0 . If $\varepsilon_g - \mu_0 < -a few kT$, then an electron with energy ε_g wouldn't be able to tunnel out into reservoir G . On the other hand, if $\varepsilon_g - \mu_0 > a few kT$, there would be no electrons in G to tunnel into the Coulomb blocked level

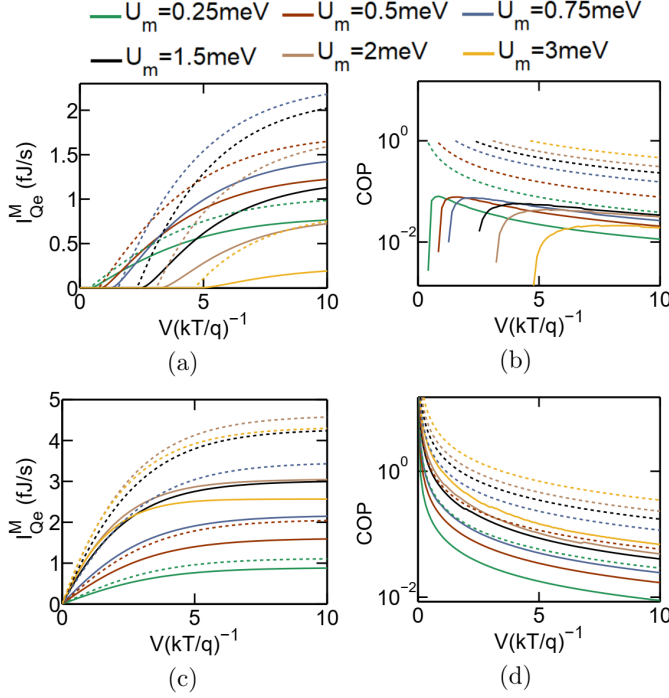


FIG. 6. Comparison of performance of the proposed design (solid Lines) with the optimal setup (dashed Lines) for different values of Coulomb coupling energy U_m with $T_L = T_R = 10K$ & $T_G = 5K$. Top panel: (a) Cooling power and (b) COP (log scale) as a function of bias voltage (V) at $T_{L(R)} = 10K$, and $T_G = 5K$. Bottom panel: (c) Cooling power and (d) COP (log scale) as a function of bias voltage (V) at $T_{L(R)} = 10K$, and $T_G = 10K$.

$\varepsilon_g + U_m$. In fact the product $f_G(\varepsilon_g + U_m)\{1 - f_G(\varepsilon_g)\}$ is maximized when $\varepsilon_g - \mu_0 = -\frac{U_m}{2}$. Since $U_m \approx -\frac{3kT}{q}$ in this case, we can note the maximum cooling power occurs around $\varepsilon_g - \mu_0 = -\frac{3kT}{2q}$. Fig. 2 (b) demonstrates the variation in COP for the low bias condition. We note a monotonic increase in COP with ε_g and ε_s^1 . Fig. 3 (a) and (b) demonstrates the cooling power and COP for high bias condition with $V = 10\frac{kT}{q}$. We note that the refrigeration engine now operates over a wide range of ε_s^1 , mainly due to the increase in the electron transport window with an increase in the applied bias V . The operation regime, in terms of ε_g , however, remains almost the identical to the low bias case. The COP , shows a similar trend with the low bias case, that is the COP increases with ε_g and ε_s^1 . By comparing Fig. 2 and Fig. 3 we note a drastic increase (about 10 times) in the maximum cooling power. This is due to the fact that an increase in bias voltage causes more electrons to flow between L and R , which increases the rate of heat absorption from G . The COP , on the other hand, decreases drastically with an applied bias voltage. This can be explained by the fact that an increase in the bias voltage causes a higher power dissipation per unit electron flow (qV) or per unit heat packet (U_m) absorption from G , which results in a

decrease in COP . It should be noted that an equivalent trend of increase in refrigeration power and decrease in overall COP with increase in bias voltage can also be noted for lower dimensional and bulk Peltier refrigerators [20, 22].

The variation of the optimal performance of the refrigeration engine with variation in the Coulomb coupling energy (U_m) and applied bias voltage is demonstrated in Fig. 4 and 5 for the cases $T_G = T_{L(R)}$ and $T_G < T_{L(R)}$ respectively. In particular, Fig. 4(a) demonstrates the maximum cooling power (I_{Qe}^M) and Fig. 4(b) demonstrates the COP at the maximum cooling power for a range of values of the applied bias voltage V and the Coulomb coupling energy (U_m). To achieve the maximum cooling power the ground states of the dots are adjusted to the optimal position, with respect to the equilibrium Fermi-energy. In Fig. 4, the maximum cooling power, as well as the COP , is low for low values of U_m . Despite of a high current for lower values of U_m [38], the total cooling power is low due to low value of the average heat extracted per unit electron flow. Due to low values of heat extracted per unit electron flow, the COP also remains low for low values of U_m . The high magnitude of current flow results in a high power dissipation despite of a lower cooling power due to lower values of U_m . As U_m increases, the net rate of electron flow decreases for the same value of bias voltage V [38]. However, the average heat extracted per unit electron flow increases with U_m . These two competing processes result in an initial increase in cooling power with an increase in U_m . With further increase in U_m beyond a certain limit, the cooling power finally decreases due to a decrease in the total current flowing through the system. From the perspective of the dot G_1 , it can be stated that the net cooling power decreases with increase in U_m beyond a certain limit due to a lower probability of electrons tunneling into the gate G_1 with an energy $\varepsilon_g + U_m$, when the ground state of S_1 is already occupied. With an increase in the applied bias V , we note a monotonic increase in the cooling power, till saturation and a deterioration in the COP . The saturation in cooling power at high values of the applied bias ($V > a \text{ few } kT/q$) occurs due to a saturation in electronic current through the system. The reasons of the decrease in COP with an increase in applied bias has already been discussed with respect to Fig. 2 and 3. Fig. 5(a) and (b) depicts the refrigeration performance of the system for $T_G < T_{L(R)}$. Here, certain differences should be noted when compared to the refrigeration performance of the system for $T_G = T_{L(R)}$. First of all, the cooling power is non-zero only when the voltage exceeds a certain minimum value, which we call the threshold voltage (V_{TH}). The threshold voltage appears due to the presence of a thermoelectric force for $T_G < T_{L(R)}$ which tends to drive electrons from R towards L , while dumping heat packets into the reservoir G [50]. Secondly, the voltage beyond which nonzero cooling power is achieved, increases with the increase in Coulomb coupling energy U_m . This again is due to the increase in

the open-circuited thermoelectric voltage in such a set-up with increase in U_m [50]. The applied bias must overcome the thermoelectric voltage to effectively cool the reservoir G . Thirdly, the maximum saturation cooling power, as well as the COP becomes much lower compared to the case of $T_G = T_{L(R)}$. In addition the cooling power at higher values of U_m becomes negligibly small. This again can be explained based on the reverse thermoelectric force acting on the system. Since the applied bias has to inject current against the reverse thermoelectric flux, we get a lower cooling power for a high bias, which, in turn, is responsible for deteriorating the COP . In other words, the regime of operation of the proposed refrigeration engine gets squeezed when $T_G < T_{L(R)}$ (demonstrated in Fig. 5a). An exhaustive discussion and analysis for the case of $T_G < T_{L(R)}$ is presented later.

Performance comparison with optimal non-local refrigeration engine: Fig. 6 demonstrates the performance comparison between the proposed design and optimal non-local refrigeration engine [1–5] for two different cases (i) $T_G < T_{L(R)}$ (top panel) and (ii) $T_G = T_{L(R)}$ (bottom panel). For performance comparison, the system to reservoir coupling of the optimal non-local refrigeration engine is taken to be $\gamma_l(\varepsilon) = \gamma_c \theta(\varepsilon_s^1 + \delta\varepsilon - \varepsilon)$, $\gamma_l(\varepsilon) = \gamma_c \theta(\varepsilon - \delta\varepsilon - \varepsilon_s^1)$ and $\gamma_g(\varepsilon) = \gamma_c$ [1–5], where $\delta\varepsilon < U_m$ and θ is Heaviside step function. The maximum cooling power (I_{Qe}^M) and COP (in log-scale) as a function of bias voltage V are plotted respectively in the left and right panel of Fig. 6 for $T_G < T_{L(R)}$ (top panel) and $T_G = T_{L(R)}$ (bottom panel) for different values of U_m . For $5K = T_G < T_{L(R)} = 10K$, the overall maximum cooling power for the optimal set-up and the proposed design are $2.1J/s$ and $1.45J/s$ respectively. The overall maximum cooling power, in both the set-ups is achieved at $U_m = 0.75meV$ ($\approx 1.75 \frac{kT_G}{q}$). Similarly, for $T_G = T_{L(R)} = 10K$, the overall maximum cooling power for the optimal set-up and the proposed set-up are $4.6J/s$ and $3J/s$ respectively. In this case, the maximum cooling power for both the set-ups occur at $U_m = 2meV$ ($\approx 2.3 \frac{kT_G}{q}$). Thus, in both the cases, the overall maximum cooling power of the proposed design hovers around 65–70% of that of the optimal set-up. Fig. 6 (b) and (d) depicts the COP (log-scale) for the proposed set-up (solid lines) and the optimal design (dashed lines) for the cases $T_G < T_{L(R)}$ and $T_G = T_{L(R)}$ respectively. We note that the COP for the proposed design is much less than that of the optimal set-up. This is because in our proposed set-up a fraction of the total number of electrons flow from L to R without absorbing heat from the reservoir G (explained in the next part).

Sequential tunneling mechanism leading to a performance degradation: Now, we discuss the sequential transport mechanisms leading to a performance degradation of the proposed refrigeration engine. Let us consider the sequence of electron transport from L to R that results in absorbing a heat packet U_m from reservoir G . For example, in the sequence $|0, 0, 0\rangle \rightarrow |1, 0, 0\rangle \rightarrow |1, 1, 0\rangle \rightarrow |0, 1, 1\rangle \rightarrow |0, 1, 0\rangle \rightarrow |0, 0, 0\rangle$, the system ini-

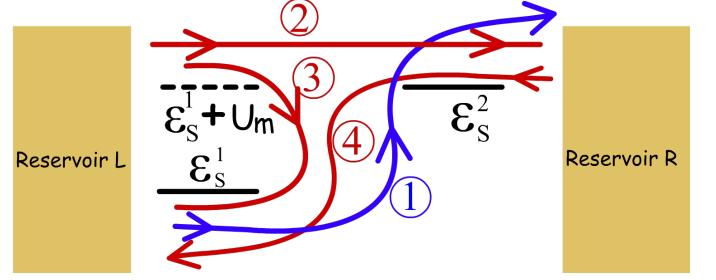


FIG. 7. Schematic diagram demonstrating the different electronic current components from the reservoir L to the system through the energy level ε_s^1 and the Coulomb blocked level $\varepsilon_s^1 + U_m$. Four current components are shown in the figure. (1) electron current flows due to voltage bias from the reservoir L to the R while absorbing a heat packet U_m (per electron) from G . (2) Electron current, due to applied bias, flows directly from L to R without any heat absorption. (3) and (4): Electron current flow due to thermoelectric force, that tends to flow while dumping heat packet U_m into the reservoir G .

tially starts with the vacuum state $|0, 0, 0\rangle$. An electron is injected from reservoir L into S_1 at energy ε_s^1 , followed by another electron injected into G_1 from G with an energy $\varepsilon_g + U_m$. This is followed by, the electron in S_1 tunneling into S_2 , after which the electron present in G_1 tunnels out into reservoir G with an energy ε_g . At the end of the cycle, the system returns to the vacuum state when the electron present in S_2 tunnels out, with energy $\varepsilon_s^2 = \varepsilon_s^1 + U_m$, into R . Thus, in the entire process illustrated above an electron is transmitted from the reservoir L to R while absorbing a heat packet U_m from G . These type of transport processes contribute to refrigeration of the target reservoir G and are illustrated as (1) in Fig. 7. The second electron transport component, depicted in Fig. 7 as (2), results in direct transmission of electrons between L and R without an absorption of heat packets from G . Hence, this component results in wastage of power, thereby causing a degradation of COP . Next, let us consider the following sequence of electron transport $|0, 0, 0\rangle \rightarrow |1, 0, 0\rangle \rightarrow |1, 1, 0\rangle \rightarrow |0, 1, 0\rangle \rightarrow |0, 0, 0\rangle$. In the above sequence, an electron tunnels, with an energy ε_s^1 , into S_1 from reservoir L . This is followed by an electron entering G_1 , from reservoir G , with an energy $\varepsilon_g + U_m$. At the next step, the electron present in S_1 tunnels out into reservoir L with an energy $\varepsilon_s^1 + U_m$. At the end of the sequence, the electron in G_1 exits into reservoir G with an energy ε_g . It is evident that in this process, a packet of heat energy U_m is transmitted from reservoir L to G . Thus, this kind of sequence results in heating up of the target reservoir G and is only positive and finite for $T_G < T_{L(R)}$ [50]. This current component, depicted in Fig. 7 as (3), flows due to thermoelectric force and affects the refrigeration performance of the proposed refrigeration engine by transmitting heat packets into G . Another thermoelectric component, that flows for $T_G < T_{L(R)}$, while dumping heat packets into G is shown as (4) in Fig. 7. From Fig. 7 and the above dis-

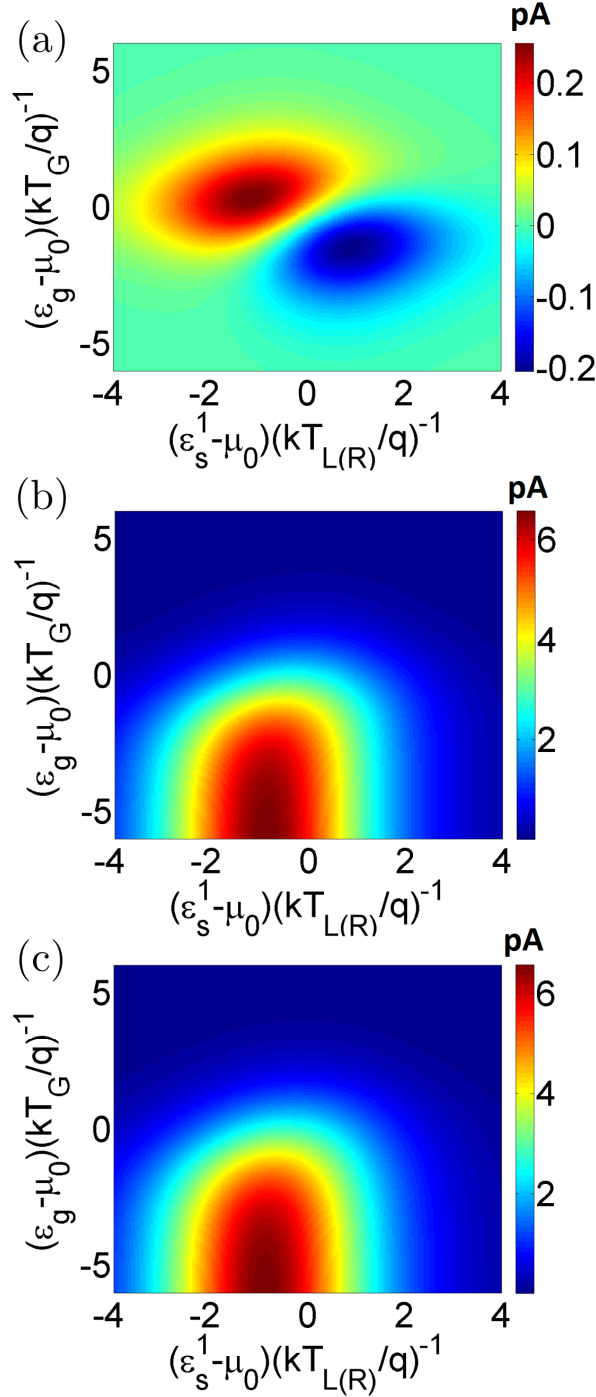


FIG. 8. Colour plots demonstrating the electron flow into the system from the reservoir L with variation in the ground states ϵ_g and ϵ_s^1 , for $U_m = 0.75 \text{ meV}$ ($\approx 1.16 \frac{kT}{q}$) and $V = 1.3 \text{ meV}$ ($\approx 2 \frac{kT}{q}$), through (a) the ground state ϵ_s^1 (b) the Coulomb blocked level $\epsilon_s^1 + U_m$. (c) Total average electron current between the system and the reservoir L .

cussions, it is clear that the electron flow components (2) and (3) from L into the Coulomb blocked level $\epsilon_s^1 + U_m$

result in degradation of the refrigeration performance.

To further elaborate the above discussion, we separate out the current flow into the system from the reservoir L as:

$$I_L = I_1 + I_2,$$

where

$$\begin{aligned} I_1 &= q\gamma_c \times \{P_{0,0}^{\epsilon_s^1} f_L(\epsilon_s^1) - P_{1,0}^{\epsilon_s^1} (1 - f_L(\epsilon_s^1))\} \\ I_2 &= q\gamma_c \{P_{0,1}^{\epsilon_s^1} f_L(\epsilon_s^1 + U_m) - P_{1,1}^{\epsilon_s^1} \{1 - f_L(\epsilon_s^1 + U_m)\}\} \end{aligned} \quad (9)$$

In the above equation, I_1 and I_2 denote the total electron current from reservoir L to the energy level ϵ_s^1 and the Coulomb blocked level $\epsilon_s^1 + U_m$ respectively. Particularly, Fig. 8(a) and (b) respectively depict the electron current flow into the system from reservoir L via the energy level ϵ_s^1 (I_1) and the Coulomb blocked level $\epsilon_s^1 + U_m$ (I_2). Fig. 8(c), on the other hand, depicts the overall electronic flow $I_L = I_1 + I_2$ from the reservoir L into the system.

We find that the electron current flow I_1 through ϵ_s^1 into the system from L is positive, over certain regime and negative over the rest. The positive regime corresponds to refrigeration of the target reservoir G . The negative regime, on the other hand, has the potential for thermoelectric generation where the flux of electrons flow against the voltage bias due to thermoelectric force [50]. The regime with negative value of I_1 corresponds to no net cooling of the target reservoir G . Interestingly, we also find that the current component I_2 through the Coulomb blocked energy level $\epsilon_s^1 + U_m$ is positive, as already shown in Fig. 8(b). This electron current constitutes the components (2) and (3). As already discussed, these current components results only in deterioration of the net cooling power, as well as, the COP . Thus, they negatively affect the refrigeration performance. The deterioration in performance of the refrigeration engine, due to these current components (2) and (3), which enter the system via the Coulomb blocked level $\epsilon_s^1 + U_m$, can be checked by adding an extra filter. Such an electron filter is to be added between L and S_1 to restrict electron flow via the Coulomb blocked level $\epsilon_s^1 + U_m$ to reduce the current components (2) and (3). However, doing so neutralizes the novelty of the proposed set-up in terms of fabrication simplicity. In Fig. 8(c), we show the total electronic current flow from L to S_1 . It is clear that a very large portion of the total electron flow actually consists of the component (2), which results in a lower COP in the proposed system compared to the optimal design.

Performance analysis for $T_G < T_{L(R)}$: For a practical electronic refrigeration engine, the target temperature of the reservoir G should generally be less than the environmental temperature or the average temperature of the current path. We have already noted that when the temperature of the target reservoir G is less than

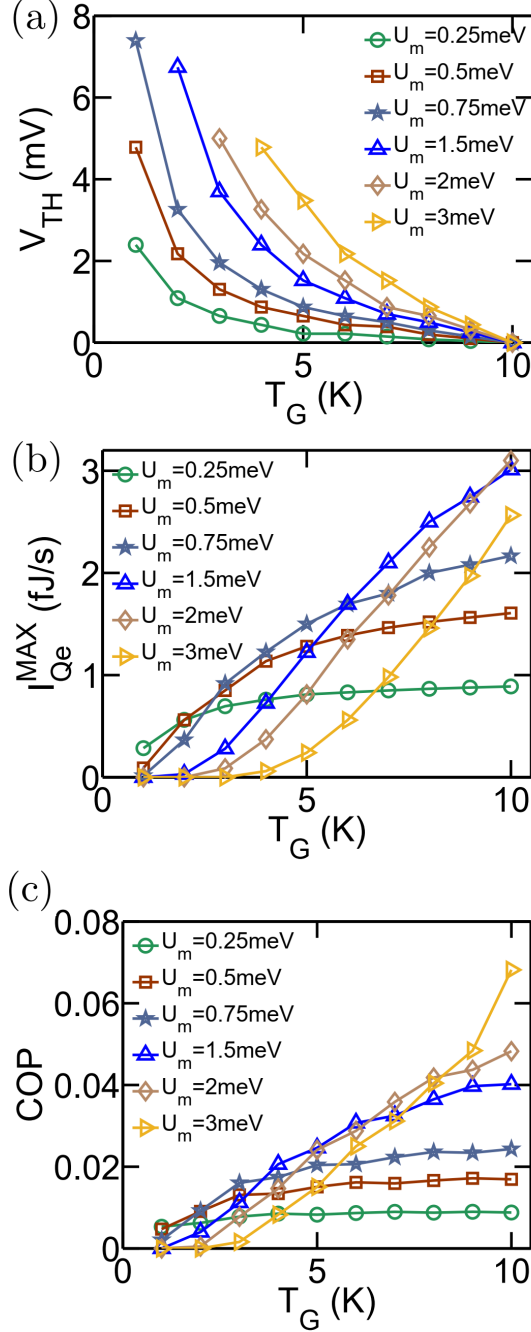


FIG. 9. Performance variation of the proposed refrigeration engine as the target temperature of the reservoir G (T_G) is gradually decreased beyond $T_{L(R)}$. Variation in (a) Threshold voltage V_{TH} (b) overall maximum cooling power I_{Qe}^{MAX} and (c) COP at the maximum cooling power (for $V = 10 \frac{kT_{L(R)}}{q}$) with decrease in the target temperature T_G of the reservoir G .

$T_{L(R)}$, the applied bias voltage needs to be greater than a certain threshold voltage V_{TH} due to reverse thermoelectric flux [50]. Fig. 9 demonstrates the performance of the proposed refrigeration engine as the temperature of reservoir G is gradually reduced below $T_{L(R)}$. Specifically,

Fig. 9(a) depicts the variation in the required threshold voltage to achieve refrigeration, while Fig. 9(b) demonstrates the variation in maximum (saturation) cooling power I_{Qe}^{MAX} with T_G for different values of U_m . From Fig. 9, we can infer a number of points on the practical conditions of operations of the refrigeration engine, depending on the target temperature of the reservoir G . We note from Fig. 9(a), that the threshold voltage V_{TH} is zero for $T_G = T_{L(R)}$ and increases with decrease in T_G . This is because the non-local thermoelectric voltage, which acts opposite to the bias voltage increases with increase in $\Delta T = T_{L(R)} - T_G$. This basically means that to achieve a lower target temperature T_G , even under ideal conditions of *zero* lattice thermal conductivity, we need to apply a higher voltage bias V . We also note that the threshold voltage V_{TH} increases with increase in U_m . This is due to an increase in the open-circuit thermoelectric voltage with an increase in U_m [50]. Fig. 9(b) demonstrates the variation in the saturation cooling power (high bias voltage limit) with a decrease in the target temperature T_G for various values of U_m . With a decrease in the target temperature the saturation cooling power decreases monotonically. An interesting point to note is that for higher values of target temperature T_G , the saturation cooling power is higher for higher values of U_m . On the other hand, when one approaches smaller target temperature T_G , the saturation cooling power is higher for lower values of U_m . In particular, we note that beyond $T_G \leq 2$ K, the saturation cooling power for $U_m \geq 1.5$ meV is approximately *zero*, which basically points out that a system with $U_m \geq 1.5$ meV cannot be employed to achieve a temperature beyond 2 K, even under ideal conditions. This can be understood by the fact that a non-zero cooling power demands finite value for both $f_G(\varepsilon_g + U_m)$ and $1 - f_G(\varepsilon_g)$, so that electrons can tunnel into G_1 with energy $\varepsilon_g + U_m$ and tunnel out into reservoir G with energy ε_g . At very low temperature, the smearing of Fermi function f_G around μ_0 decreases significantly, making the product $f_G(\varepsilon_g + U_m)\{1 - f_G(\varepsilon_g)\} \approx 0$ for any ε_g at higher values of U_m . Hence, at lower target temperature T_G , the saturation or maximum value of cooling power becomes approximately zero for higher values of U_m . Thus for higher values of U_m , even by applying a high bias voltage, we cannot achieve a target temperature T_G lower than a certain minimum temperature (since the saturation cooling power becomes zero beyond a certain minimum temperature). We hence conclude that even under ideal conditions, depending on the Coulomb coupling energy U_m , there is a minimum limit beyond which the target temperature T_G cannot be reduced. So, for achieving a lower target temperature T_G , one needs to design a system with lower value of U_m and operate it at a higher value of bias voltage V . Fig. 9(c) demonstrates the variation of COP with target reservoir temperature at the maximum cooling power for $V = \frac{10kT}{q}$. We note that there is fall in COP as one approaches lower target reservoir temperature, the fall being more sharper for higher values of U_m . This is

because a higher magnitude of U_m results in a higher value of the open-circuit thermoelectric voltage as one approaches lower values of target reservoir temperature. A higher thermoelectric voltage, acting opposite to the bias voltage, results in a sharper decrease in COP with fall in the target reservoir temperature for higher values of U_m . Although not demonstrated in this paper, in the case of $T_G > T_{L(R)}$, the target reservoir G is automatically cooled (without an applied bias voltage) with T_G gradually approaching $T_{L(R)}$, due to the presence of a thermoelectric force that tends to drive a current between L and R while extracting heat from reservoir G [50].

IV. CONCLUSION

In this paper, we have proposed a realistic design for non-local refrigeration engine based on Coulomb coupled systems. The performance of the proposed refrigeration engine was then theoretically investigated employing the quantum master equation (QME) formalism. It was demonstrated that the maximum cooling power of

the proposed set-up hovers around 65 – 70% of the optimal design proposed in literature [1–5]. Despite a lower cooling power, the key edge of the proposed set-up over the optimal design is the integration of fabrication simplicity along with decent refrigeration performance. In our discussions, we have restricted transport phenomena in the weak coupling regime, so that co-tunneling processes can be neglected. The refrigeration power in the proposed set-up can be enhanced by a few orders by tuning electronic transport in the regime of strong coupling, that is by enhancing the system-to-reservoir and the interdot tunnel coupling. An analysis on the effects of cotunneling and higher order processes on the refrigeration performance of the proposed system constitutes an interesting aspect of investigation. Furthermore, an analysis of the impact of electron-phonon scattering [23–34] on the performance of the proposed refrigeration engine also constitutes an interesting aspect of future research. The various possible designs for non-local refrigeration systems is left for future investigation. Nevertheless, the design demonstrated here can be used to realize high performance non-local cryogenic refrigeration engines employing Coulomb coupled systems.

-
- [1] P. A. Erdman, B. Bhandari, R. Fazio, J. P. Pekola, and F. Taddei, *Phys. Rev. B* **98**, 045433 (2018).
 - [2] A.-M. Daré, *Phys. Rev. B* **100**, 195427 (2019).
 - [3] Y. Zhang and J. Chen, *Physica E: Low-dimensional Systems and Nanostructures* **114**, 113635 (2019).
 - [4] R. Sánchez, H. Thierschmann, and L. W. Molenkamp, *New Journal of Physics* **19**, 113040 (2017).
 - [5] Y. Zhang, G. Lin, and J. Chen, *Phys. Rev. E* **91**, 052118 (2015).
 - [6] G. J. Snyder, E. S. Toberer, R. Khanna, and W. Seifert, *Phys. Rev. B* **86**, 045202 (2012).
 - [7] Y. Apertet, H. Ouerdane, A. Michot, C. Goupil, and P. Lecoeur, *EPL (Europhysics Letters)* **103**, 40001 (2013).
 - [8] A. Shakouri and J. E. Bowers, *Applied Physics Letters* **71**, 1234 (1997).
 - [9] A. Shakouri, E. Y. Lee, D. L. Smith, V. Narayanamurti, and J. E. Bowers, *Microscale Thermophysical Engineering* **2**, 37 (1998).
 - [10] X. Fan, G. Zeng, E. Croke, G. Robinson, C. LaBounty, A. Shakouri, and J. E. Bowers, in *ITHERM 2000. The Seventh Intersociety Conference on Thermal and Thermomechanical Phenomena in Electronic Systems (Cat. No. 00CH37069)*, Vol. 1 (2000) p. 307.
 - [11] X. Fan, G. Zeng, E. Croke, C. LaBounty, D. Vashaee, A. Shakouri, and J. E. Bowers, *Electronics Letters* **37**, 126 (2001).
 - [12] R. Kim, C. Jeong, and M. S. Lundstrom, *Journal of Applied Physics* **107**, 054502 (2010).
 - [13] J. p. Zhu and G. x. Li, *Phys. Rev. A* **86**, 053828 (2012).
 - [14] Z.-Z. Li, S.-H. Ouyang, C.-H. Lam, and J. Q. You, *EPL (Europhysics Letters)* **95**, 40003 (2011).
 - [15] F. Giazotto, T. T. Heikkilä, A. Luukanen, A. M. Savin, and J. P. Pekola, *Rev. Mod. Phys.* **78**, 217 (2006).
 - [16] H. L. Edwards, Q. Niu, and A. L. de Lozanne, *Applied Physics Letters* **63**, 1815 (1993).
 - [17] K. A. Chao, M. Larsson, and A. G. Malshukov, *Applied Physics Letters* **87**, 022103 (2005).
 - [18] R. S. Whitney, *Physical Review Letters* **112**, 130601 (2014).
 - [19] R. S. Whitney, *Phys. Rev. B* **91**, 115425 (2015).
 - [20] A. Singha, *Physics Letters A* **382**, 3026 (2018).
 - [21] R. Kim, C. Jeong, and M. S. Lundstrom, *Journal of Applied Physics* **107**, 054502 (2010).
 - [22] A. Singha and B. Muralidharan, *Journal of Applied Physics* **124**, 144901 (2018).
 - [23] N. Mingo and D. A. Broido, *Phys. Rev. Lett.* **93**, 246106 (2004).
 - [24] N. Mingo, *Applied Physics Letters* **84**, 2652 (2004).
 - [25] F. Zhou, J. Szczech, M. T. Pettes, A. L. Moore, S. Jin, and L. Shi, *Nano Letters* **7**, 1649 (2007), pMID: 17508772.
 - [26] F. Zhou, A. L. Moore, M. T. Pettes, Y. Lee, J. H. Seol, Q. L. Ye, L. Rabenberg, and L. Shi, *Journal of Physics D: Applied Physics* **43**, 025406 (2010).
 - [27] A. I. Boukai, Y. Bunimovich, J. Tahir-Kheli, J.-K. Yu, W. A. Goddard, and J. R. Heath, *Nature* **451**, 168 (2008).
 - [28] A. I. Hochbaum, R. Chen, R. D. Delgado, W. Liang, E. C. Garnett, M. Najarian, A. Majumdar, and P. Yang, *Nature Publishing Group* **451**, 163 (2008).
 - [29] A. Balandin, A. Khitun, J. Liu, K. Wang, T. Borca-Tasciuc, and G. Chen, in *Eighteenth International Conference on Thermoelectrics* (1999) pp. 189–192.
 - [30] G. Chen, *Phys. Rev. B* **57**, 14958 (1998).
 - [31] T. Koga, S. B. Cronin, M. S. Dresselhaus, J. L. Liu, and K. L. Wang, *Applied Physics Letters* **77** (2000).

- [32] B. L. Davis and M. I. Hussein, *Phys. Rev. Lett.* **112**, 055505 (2014).
- [33] Y. Pan, G. Hong, S. N. Raja, S. Zimmermann, M. K. Tiwari, and D. Poulikakos, *Applied Physics Letters* **106**, 093102 (2015).
- [34] J. P. Feser, J. S. Sadhu, B. P. Azeredo, K. H. Hsu, J. Ma, J. Kim, M. Seong, N. X. Fang, X. Li, P. M. Ferreira, S. Sinha, and D. G. Cahill, *Journal of Applied Physics* **112**, 114306 (2012).
- [35] K. Uchida, H. Adachi, T. Kikkawa, A. Kirihara, M. Ishida, S. Yoroza, S. Maekawa, and E. Saitoh, *Proceedings of the IEEE* **104**, 1946 (2016).
- [36] J. Sinova, S. O. Valenzuela, J. Wunderlich, C. H. Back, and T. Jungwirth, *Rev. Mod. Phys.* **87**, 1213 (2015).
- [37] E. Saitoh, M. Ueda, H. Miyajima, and G. Tatara, *Applied Physics Letters* **88**, 182509 (2006).
- [38] A. Singha, “Density matrix to quantum master equation (qme) model for arrays of coulomb coupled quantum dots in the sequential tunneling regime,” (2020), [arXiv:2003.00522 \[physics.app-ph\]](https://arxiv.org/abs/2003.00522).
- [39] K. Eng, T. D. Ladd, A. Smith, M. G. Borselli, A. A. Kiselev, B. H. Fong, K. S. Holabird, T. M. Hazard, B. Huang, P. W. Deelman, I. Milosavljevic, A. E. Schmitz, R. S. Ross, M. F. Gyure, and A. T. Hunter, *1* (2015), [10.1126/sciadv.1500214](https://doi.org/10.1126/sciadv.1500214).
- [40] H. Flentje, B. Bertrand, P.-A. Mortemousque, V. Thiney, A. Ludwig, A. D. Wieck, C. Buerle, and T. Meunier, *Applied Physics Letters* **110**, 233101 (2017).
- [41] F. N. M. Froning, M. K. Rehmann, J. Ridderbos, M. Brauns, F. A. Zwanenburg, A. Li, E. P. A. M. Bakkers, D. M. Zumbühl, and F. R. Braakman, *Applied Physics Letters* **113**, 073102 (2018).
- [42] A. Noiri, K. Kawasaki, T. Otsuka, T. Nakajima, J. Yoneda, S. Amaha, M. R. Delbecq, K. Takeda, G. Allison, A. Ludwig, A. D. Wieck, and S. Tarucha, *Semiconductor Science and Technology* **32**, 084004 (2017).
- [43] C. Hong, G. Yoo, J. Park, M.-K. Cho, Y. Chung, H.-S. Sim, D. Kim, H. Choi, V. Umansky, and D. Mahalu, *Phys. Rev. B* **97**, 241115 (2018).
- [44] T. Takakura, A. Noiri, T. Obata, T. Otsuka, J. Yoneda, K. Yoshida, and S. Tarucha, *Applied Physics Letters* **104**, 113109 (2014).
- [45] A. Hbel, J. Weis, W. Dietsche, and K. v. Klitzing, *Applied Physics Letters* **91**, 102101 (2007).
- [46] I. H. Chan, R. M. Westervelt, K. D. Maranowski, and A. C. Gossard, *Applied Physics Letters* **80**, 1818 (2002).
- [47] L. W. Molenkamp, K. Flensberg, and M. Kemerink, *Phys. Rev. Lett.* **75**, 4282 (1995).
- [48] A. Hbel, J. Weis, W. Dietsche, and K. v. Klitzing, *Applied Physics Letters* **91**, 102101 (2007), <https://doi.org/10.1063/1.2778542>.
- [49] I. M. Ruzin, V. Chandrasekhar, E. I. Levin, and L. I. Glazman, *Phys. Rev. B* **45**, 13469 (1992).
- [50] A. Singha, “A realistic non-local heat engine based on coulomb coupled systems,” (2020), [arXiv:2003.03023 \[physics.app-ph\]](https://arxiv.org/abs/2003.03023).
- [51] S. Datta, *Quantum Transport: Atom to Transistor* (Cambridge Press, 2005).